PHYSICAL REVIEW VOLUME 163, NUMBER 4 20 NOVEMBER 1967

Inelastic Scattering of 40-MeV Polarized Protons*†

M. P. Fricke,‡ E. E. Gross, and A. Zucker
Oak Ridge National Laboratory, Oak Ridge, Tennessee

(Received 5 July 1967)

The left-right asymmetry and differential cross section for the inelastic scattering of 40-MeV polarized protons were measured over a large angular region for each of the following 2^+ excitations: 1.78 MeV in ^{28}Si, 1.41 and 2.97 MeV in ^{54}Fe, 1.45 MeV in ^{58}Ni, and 1.33 MeV in ^{60}Ni. Some asymmetry and cross-section data were also obtained for 3^- states: 6.9 MeV in ^{28}Si, 4.8 and 6.4 MeV in ^{54}Fe, 4.5 MeV in ^{58}Ni, and 4.08 MeV in ^{60}Ni. The inelastic scattering was analyzed in the distorted-wave approximation, using the collective-model extension of the optical-model potential determined by fitting elastic polarization and cross-section measurements for each target. The inelastic asymmetry and cross-section data are best reproduced with a collective-model interaction obtained by deforming the complete optical potential, including its imaginary and spin-orbit parts.

I. INTRODUCTION

In recent years, a large number of cross sections for the inelastic scattering of 8- to 55-MeV protons has been analyzed[1–3] assuming a collective-model generalization of the optical model.[4–6] In this treatment, the optical-model potential found to reproduce the observed elastic scattering is made nonspherical, and the nonspherical part induces transitions to vibrational or rotational states of the target nucleus. The free parameters in the model are the multipole order l of the transition and its strength, or deformation parameter β_l; these are deduced by comparison to the shape and magnitude, respectively, of the measured differential cross section. Data for low-lying 2^+ and 3^- states in even-mass nuclei have been successfully reproduced by assuming a simple, single-step excitation appropriate for a 2^l-pole rotation or single-phonon surface oscillation. Unless the coupling between the ground and excited states is uncommonly strong,[7] such transitions induced by medium-energy protons can be treated in the distorted-wave approximation.[5,6]

At present it appears that measurements of the polarization in inelastic proton scattering, or of the left-right asymmetry in the inelastic scattering of a polarized beam, can contribute to our understanding of this reaction in several ways. Perhaps the simplest question which can be answered by such experiments is whether or not the data for low-lying excitations are reproduced by the collective-model calculation found so successful for the cross sections. The cross sections have seemed well described by a deformation of the central part of the optical potential and have presented no obvious demand for a spin-dependent term in the nonspherical interaction. It is of interest to see if the asymmetries require a spin dependence of the form implied in the collective-model approach, that obtained by deforming also the noncentral, $\boldsymbol{\sigma}\cdot\mathbf{l}$ part of the optical potential. However, the relevance of inelastic-asymmetry measurements is not limited to questions of the proper spin dependence for the effective interaction. For example, our results present a strong demand for complex coupling, in which both real and imaginary parts of the central optical potential contribute to the nonspherical interaction.[8] Also, the inelastic-asymmetry calculations are quite sensitive to the optical-model parameters, through both the elastic distortion and the collective-model interaction. Analysis of the present inelastic-asymmetry data has required a further study of the elastic data for these targets, and the optical-model parameters found are somewhat different from the latest 40-MeV results.[9] The new parameters simultaneously improve the agreement with both the elastic polarization and the inelastic asymmetry.

---

* Research sponsored by the U. S. Atomic Energy Commission under contract with the Union Carbide Corporation.

† Results of this work were submitted by one of us (MPF) in partial fulfillment of the requirements for a Ph.D. degree, University of Minnesota.

‡ Oak Ridge Graduate Fellow from the University of Minnesota under appointment from Oak Ridge Associated Universities. Present address: Cyclotron Laboratory, University of Michigan, Ann Arbor, Michigan.

[1] B. Buck, Phys. Rev. **130**, 712 (1963); F. G. Perey, R. J. Silva, and G. R. Satchler, Phys. Letters **4**, 25 (1963); G. R. Satchler, R. H. Bassel, and R. M. Drisko, *ibid.* **5**, 256 (1963); J. K. Dickens, F. G. Perey, R. J. Silva, and T. Tamura, *ibid.* **6**, 53 (1963); M. Sakai *et al.*, *ibid.* **8**, 197 (1964); K. Yagi *et al.*, *ibid.* **10**, 186 (1964); J. Benveniste, A. C. Mitchell, B. Buck, and C. B. Fulmer, Phys. Rev. **133**, B323 (1964); T. Tamura, in Argonne National Laboratory Report No. 6848, 1964, p. 24 (unpublished); M. P. Fricke, *ibid.*, p. 130; M. Sakai and T. Tamura, Phys. Letters **10**, 323 (1964); G. C. Pramila, R. Middleton, T. Tamura, and G. R. Satchler, Nucl. Phys. **61**, 448 (1965); R. L. Robinson, J. L. C. Ford, Jr., P. H. Stelson, and G. R. Satchler, Phys. Rev. **146**, 816 (1966); R. K. Cole, C. N. Waddell, R. R. Dittman, and H. S. Sandhu, Nucl. Phys. **75**, 241 (1966); J. Stevens, H. F. Lutz, and S. F. Eccles, *ibid.* **76**, 129 (1966); A. Scott and M. P. Fricke, Phys. Letters **20**, 654 (1966); J. Saudinos, G. Vallois, O. Beer, M. Gendrot, and P. Lopato, *ibid.* **22**, 492 (1966); A. L. McCarthy and G. M. Crawley, Phys. Rev. **150**, 935 (1966).

[2] S. F. Eccles, H. F. Lutz, and V. A. Madsen, Phys. Rev. **141**, 1067 (1966).

[3] M. P. Fricke and G. R. Satchler, Phys. Rev. **139**, B567 (1965).

[4] S. Hayakawa and S. Yoshida, Progr. Theoret. Phys. (Kyoto) **14**, 1 (1955); D. M. Brink, Proc. Phys. Soc. (London) **68A**, 994 (1955); J. S. Blair, Phys. Rev. **115**, 928 (1959); E. Rost and N. Austern, *ibid.* **120**, 1375 (1960).

[5] R. H. Bassel, G. R. Satchler, R. M. Drisko, and E. Rost, Phys. Rev. **128**, 2693 (1962).

[6] G. R. Satchler, Nucl. Phys. **55**, 1 (1964).

[7] F. G. Perey and G. R. Satchler, Phys. Letters **5**, 212 (1963).

[8] E. R. Flynn and R. H. Bassel, Phys. Rev. Letters **15**, 168 (1965), and references therein.

[9] M. P. Fricke, E. E. Gross, B. J. Morton, and A. Zucker, Phys. Rev. **156**, 1207 (1967).

The first measurements of inelastic asymmetries for medium-energy protons are now coming into existence. In the past year or so, inelastic-asymmetry data have been presented for the 4.43-MeV (2^+) state in ^{12}C for protons of energy 16.5 MeV,[10] 20–28 MeV,[11] and 30,[12] 40,[13] and 50 MeV,[12] and for the 1.78-MeV (2^+) state in ^{28}Si at 30 and 50 MeV.[12] Data for 2^+ states in heavier targets have been recently obtained at Saclay for 16.5- and 18.6-MeV protons. The 1.33-MeV excitation in ^{60}Ni and the 1.17-MeV excitation in ^{62}Ni were measured[10] at 16.5 MeV; and the following excitations were observed[14] at 18.6 MeV: 0.99 MeV in ^{48}Ti, 1.57 MeV in ^{50}Ti, 1.43 MeV in ^{52}Cr, 1.41 and 2.97 MeV in ^{54}Fe, and 0.84 MeV in ^{56}Fe. Collective-model calculations have been made for the carbon and silicon data at 30 and 50 MeV,[12] and for the nickel data at 16.5 MeV.[15]

The work reported here presents 40-MeV proton asymmetry measurements at the Oak Ridge Isochronous Cyclotron (ORIC) for the 2^+ states at 1.78 MeV in ^{28}Si, 1.41 and 2.97 MeV in ^{54}Fe, 1.45 MeV in ^{58}Ni, and 1.33 MeV in ^{60}Ni. Some asymmetry data were also obtained for 3^- excitations at 6.9 MeV in ^{28}Si, 6.4 MeV in ^{54}Fe, 4.5 MeV in ^{58}Ni, and 4.08 MeV in ^{60}Ni. The inelastic cross section was obtained for each of these states and for the 4.8-MeV (3^-) level in ^{54}Fe. Preliminary results of the present measurements and their analysis have been reported previously[16,17] at various stages of the project. The elastic polarizations and cross sections for these targets were also obtained, and have been reported elsewhere.[9] The elastic data are discussed here only insofar as they relate to the measurement and analysis of the inelastic scattering.

II. EXPERIMENT

The equipment used in this experiment has previously[9,13,18] been described in detail. The proton beam from the ORIC cyclotron is polarized externally by elastic scattering from calcium. The scattered beam is magnetically analyzed[9] and transported to a scattering chamber equipped with 32 NaI(Tl) photomultiplier counters[18] arranged symmetrically on both sides of the beam. The polarized beam is focused to a spot on the target 4 mm wide by 11 mm high with an angular spread of ±2° in the scattering plane. The beam there has a polarization of $27.4\pm0.5\%$,[9] an intensity of 10^8 protons/sec, and an adjustable energy spread of 300–500 keV, full width at half-maximum (FWHM).

The photomultiplier outputs are routed through a shaping amplifier to a 20 000-channel pulse-height analyzer, used effectively as thirty-two 400-channel analyzers.[18] Some typical spectra from the analyzer are shown in Fig. 1. These were taken with an over-all resolution of about 750-keV FWHM, with contributions of approximately 500 keV from the energy spread in the beam and 500 keV from the detectors. The resolution can be improved by narrowing the slits of the magnet used to analyze the proton beam and by reducing the apertures of collimators used in front of the 1-in.-diam NaI scintillation crystals. This results in an over-all resolution of about 500 keV, as is illustrated with a ^{60}Ni spectrum in Fig. 2. The smaller counter apertures ($\frac{1}{8}$-in. diam) have an area 22.6 times less than the larger apertures ($\frac{3}{8}$ in. by $\frac{3}{4}$ in.) but were used at forward angles for some of the inelastic-scattering data where the reduced count rate could be tolerated.

The targets were in the range 20 to 30 mg/cm^2 in thickness, and at back angles the over-all resolution is increased to about 1 MeV due to the passage of the scattered beam back through the target. The ^{28}Si target was made of natural (92.21% ^{28}Si) high-purity silicon and was 32.1 mg/cm^2 thick. The ^{54}Fe target was 97.4% enriched and 18.0 mg/cm^2 thick. The ^{58}Ni target was 99.95% enriched and 29.95 mg/cm^2 thick, and ^{60}Ni was 99.1% enriched and 19.7 mg/cm^2 thick. The targets were all about 2 in. tall by $\frac{3}{4}$ in. wide, and their thickness at the center (where the beam is focused) could not be confidently deduced from the total weight and area of the foil. In order to normalize the cross-section measurements, thin targets (about 5 mg/cm^2) of ^{54}Fe, ^{58}Ni, and ^{60}Ni were also used to measure the elastic scattering. The thicknesses of the thin targets at their centers were determined by scanning them with a collimated, 5.48-MeV, α-particle beam from ^{241}Am and measuring the energy loss with a solid-state counter. The average of these α thickness values measured over the entire surface of each thin target was also compared to its weight-area thickness value and found to agree within the accuracy of the α measurements. The thick Si target was destroyed, and its thickness at the center was obtained by measuring the weight and area of the fragments. The precision of the thickness measurement is estimated to be ±5% for all targets.

A. Running Procedures

We now indicate the procedures used routinely to accumulate the present asymmetry and cross-section

---

[10] P. Darriulat, J. M. Fowler, R. de Swiniarski, and J. Thirion, in *Proceedings of the Second International Symposium on Polarization Phenomena of Nucleons, Karlsruhe, 1965*, edited by P. Huber and H. Schopper (Birkhäuser Verlag, Basel, Germany, 1966), p. 342.

[11] R. M. Craig, J. C. Dore, G. W. Greenlees, J. Lowe, and D. L. Watson, Nucl. Phys. **79**, 177 (1966).

[12] R. M. Craig, J. C. Dore, G. W. Greenlees, J. Lowe, and D. L. Watson, Nucl. Phys. **83**, 493 (1966).

[13] L. N. Blumberg, E. E. Gross, A. van der Woude, A. Zucker, and R. H. Bassel, Phys. Rev. **147**, 812 (1966).

[14] A. Garin, C. Glashausser, A. Papineau, R. de Swiniarski, and J. Thirion, Phys. Letters **21**, 73 (1966).

[15] F. G. Perey, in *Proceedings of the Second International Symposium on Polarization Phenomena of Nucleons, Karlsruhe, 1965*, edited by P. Huber and H. Schopper (Birkhäuser Verlag, Basel, Germany, 1966), p. 191.

[16] M. P. Fricke, R. M. Drisko, R. H. Bassel, E. E. Gross, B. J. Morton, and A. Zucker, Phys. Rev. Letters **16**, 746 (1966).

[17] M. P. Fricke, E. E. Gross, B. J. Morton, and A. Zucker, in *Proceedings of the International Conference on Nuclear Physics, Gatlinburg, Tennessee, 1966* (Academic Press Inc., New York, 1967).

[18] L. N. Blumberg, E. E. Gross, A. van der Woude, and A. Zucker, Nucl. Instr. Methods **39**, 125 (1966).

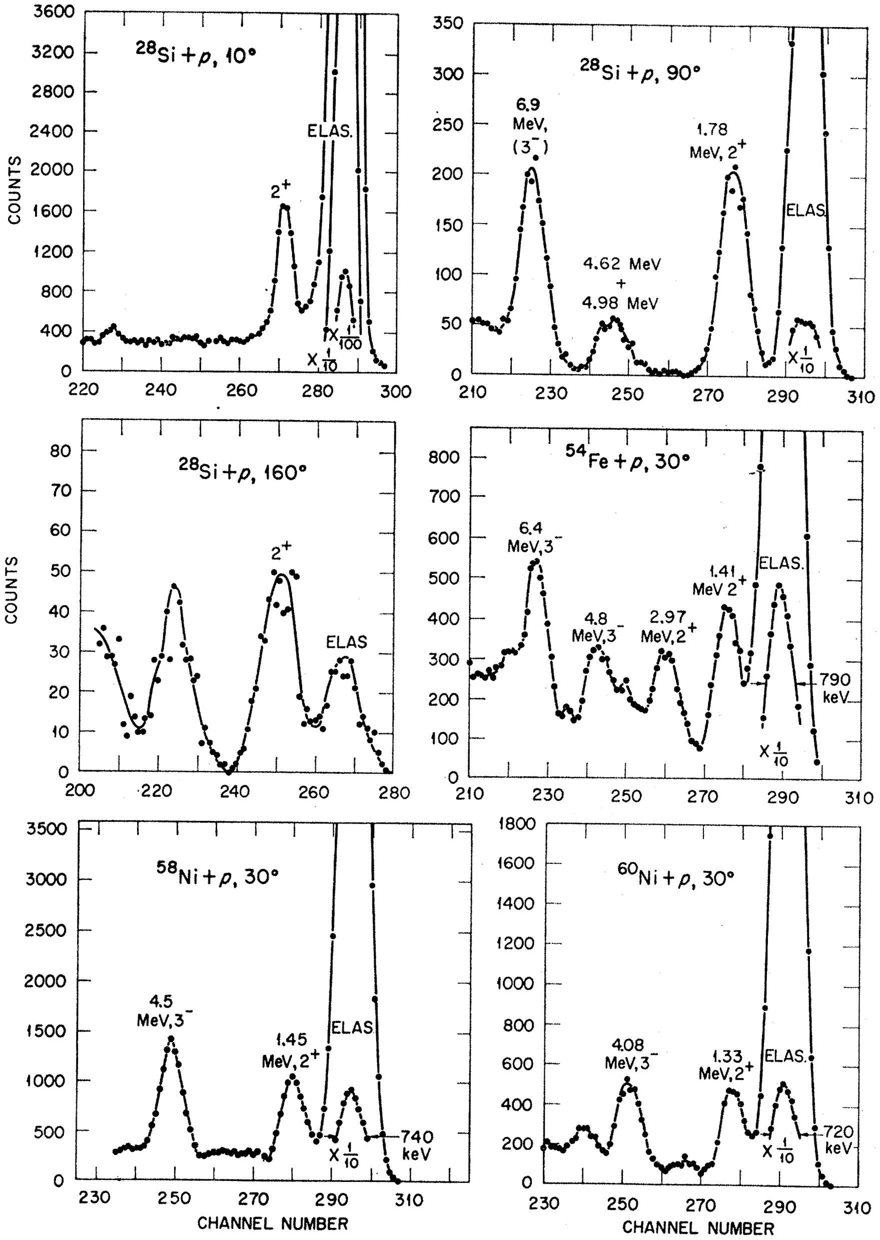

FIG. 1. Proton energy spectra with over-all resolution of 750 keV.

data; further details of the methods are given in Refs. 9 and 13. The polarized beam was first focused and centered in the scattering chamber. The energy of the beam was then determined by scattering from ^{208}Pb and measuring the pulse-height variation of the elastic peak for different thicknesses of Al absorber placed before a counter at 10°. The result of this measurement could be obtained rapidly and used to adjust the cyclotron frequency to attain the desired energy. The energy was also measured at the end of each running period by residual range in an emulsion; the constancy of the beam energy during the runs is verified by the constant field maintained in the analyzing magnet. As a result, we can state that all of the asymmetry and cross-

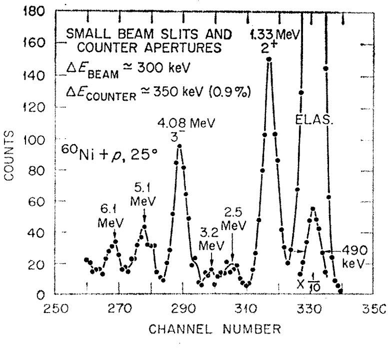

FIG. 2. Energy spectrum from ^{60}Ni with over-all resolution of 500 keV.

section data presented here were obtained with protons of energy 40.0±0.4 MeV.

The angular alignment of the counter banks on each side of the beam was checked by positioning the most forward counters at 10° on both the left and right sides and observing the asymmetry in the elastic scattering from ^{208}Pb. The angular positions of the other 15 counter apertures on each side of the beam are fixed relative to these first counters, at intervals of 10.00° ±0.05°. The slope of the differential cross section at 10° is such that a 0.1° misalignment of the counters relative to the average beam direction produces a spurious difference of 8% between the number of protons elastically scattered to the left and right sides of the beam. The angular orientation of the counters can therefore be quickly adjusted to agree with the beam direction to within ±0.05°. The alignment was checked in this way before and after each individual asymmetry run (each accumulation of data) and was never found to differ by more than this amount. During the asymmetry runs, the position and alignment of the beam were monitored with a split ion chamber located at the exit of the scattering chamber, directly in front of the Faraday cup. This ion chamber is sensitive to a 0.01-in. transverse movement of the beam from its correct position.

The elastic polarization for ^{12}C is known accurately at 40 MeV, and elastic-asymmetry data for this target were taken sometime during each running period in order to check the polarization of the beam. Using the value 70.8±1.8% for the polarization from ^{12}C at 65° lab,[9] our beam polarization in each run was found to be 27.4±0.5%.

The asymmetry was measured at 5° intervals, generally over the range 10°–165°. Elastic and inelastic data were obtained simultaneously in four 6-h runs for each target. Small counter collimators ($\frac{1}{8}$-in. diam) were used at forward angles out to an angle where the number of counts in the inelastic groups was comparable to that obtained at back angles where the large collimators ($\frac{3}{8}$ in.$\times\frac{3}{4}$ in) were used. Separate asymmetry data were taken for the targets ^{28}Si and ^{60}Ni to optimize the energy resolution at forward angles by using exclusively the smaller collimators. These data for ^{28}Si extend from 10° to 67.5° in 2.5° intervals, and for ^{60}Ni from 20° to 65° in 5° intervals. The improved resolution reduced the uncertainties in this region by about 50%.

While the asymmetry runs yielded cross sections by averaging the counts for scattering to the left and right, better elastic cross-section data, and some inelastic data at forward angles, could be easily obtained by using the counter array in the direct, unpolarized beam. There, the beam spread is only 250 keV, and the intensity is copious, so that the smaller counter collimators could be used out to back angles and the data taken at more angles. The over-all angular resolution is also improved from ±2.5° to ±1°. Elastic cross-section data from 10° to 170° in 2.5° intervals, and inelastic cross-section data from 20° to 70° in 5° intervals were obtained in about 12 h for each target.

The energies of the inelastic proton groups were established relative to the elastic scattering by a pulser calibration of the detector electronics, and the Q values were thereby determined to an accuracy of ±200 keV. Within this margin, the energies of the levels we observe are in agreement with those given in *Nuclear Data Sheets* and with those determined by Stovall and Hintz.[19] We use these two sources to assign the energies, except for the excitation we observe near 6.9 MeV in ^{28}Si, which we only tentatively identify as the known octupole excitation at 6.88 MeV.

B. Data Reduction

The data from the pulse-height analyzer were read out onto magnetic tape and processed with a small computer to obtain plots of the number of counts versus proton energy for each counter.[18] In order to unfold the spectra carefully in the region of the tails of the elastic and inelastic proton peaks, a semilogarithmic plot of the spectra was most useful. By examining a large number of spectra from different counters for ^{12}C, where the elastic and inelastic peaks are well separated, it was established that the elastic peak shape in a semilogarithmic plot is consistently and precisely repeated in the inelastic peaks. The spectra could therefore be unfolded by making successive approximations to the peak shape until the elastic and inelastic peaks agreed in shape and would account for the total counts observed, within statistics and in view of other nearby proton groups which were not resolved. No significant elastic peaks from contaminants were observed in these spectra taken with thick (20–30 mg/cm^2) targets.

An absolute elastic cross section was determined from the "cross-section runs" for each target, the runs made separately with an unpolarized beam. Using the relative elastic cross sections deduced from the asymmetry data by summing the scattering on each side of the beam, the normalization of the inelastic cross sections obtained from the asymmetry runs was then determined relative to this absolute elastic cross section. Some inelastic data from the cross-section runs were used to augment the cross sections deduced from the asymmetry runs. The elastic cross-section data obtained from the asymmetry runs, however, were used solely to normalize the inelastic cross sections to the elastic data. This and other redundancies in the elastic and inelastic data, taken at different times and in different ways, afforded a considerable number of consistency checks for these measurements.

The effect of isotopic impurities requires no correction in the elastic and inelastic data for ^{54}Fe, ^{58}Ni, and ^{60}Ni, primarily because of the high isotopic purity of these targets. The natural Si target, however, contains 4.7%

---

[19] T. Stovall and N. M. Hintz, Phys. Rev. **135**, B330 (1964).

^{29}Si and 3.09% ^{30}Si, both of which have excited states that make an uncertain contribution to the observed proton groups from ^{28}Si. The normalization of the inelastic data for ^{28}Si was therefore increased by a factor of 1.039, which is half-way between assuming no inelastic contributions from the adjacent isotopes, and, at the other extreme, assuming that all the isotopes have a state at the same energy with equal strength. An additional normalization uncertainty of ±4% is added for the inelastic cross-section data from ^{28}Si to bracket these possibilities. All absolute cross sections were corrected by a factor of 1.023 to account for the loss of counts due to reactions undergone by the scattered protons in the NaI crystal. This factor was deduced from the work of Measday[20] for our method of unfolding the proton spectra, in which we do not include the tails of the peaks below about 1 MeV from their maxima.

Our inelastic asymmetry results $\epsilon(\theta)$ are normalized to 100% beam polarization using

$$\epsilon(\theta)=\frac{1}{P_B}\frac{N_L(\theta)-N_R(\theta)}{N_L(\theta)+N_R(\theta)}. \tag{1}$$

Here N_L is the number of protons scattered to the left, and N_R the number scattered to the right, with left such that $\mathbf{k}_i\times\mathbf{k}_f$ is in the direction of the beam polarization (Basel convention). The actual beam polarization P_B is 0.274.

The total absolute error in the normalization of the cross-section data is taken to be an uncorrelated combination of the uncertainty in target thickness (±5%), solid angle (±1%), beam integration (±2%), and, for the inelastic results for ^{28}Si, isotopic impurities (±4%). The absolute error for the elastic cross sections, and for the inelastic cross sections for iron and nickel, is then ±5.5%, and that for the inelastic silicon data is ±6.8%. The absolute error in the normalization of the asymmetries is taken to be that due to the uncertainty in beam polarization, ±1.8% of the value of ϵ.

The relative probable errors in the cross-section and asymmetry data stem mainly from uncertainties in unfolding the energy spectra and from statistics. These are assumed uncorrelated, so that the total error $\pm\Delta N$ in the net counts in a peak is given by

$$\Delta N^2=\Delta N_0^2+\Delta N_B^2+\Delta N_S^2. \tag{2}$$

The error ΔN_0 is the estimated uncertainty of the counts assigned to the peak in the region where it overlaps adjacent peaks, and ΔN_B is the uncertainty in any background under an inelastic peak due primarily to the tail of the elastic peak. The error ΔN_S is the total statistical error, including contributions from N_0 and N_B. Typically, ΔN_0 was judged to be 30% of the total contribution to the peak in an overlapping region, and ΔN_B amounted to 20% of the total background under the peak. ΔN_B was a major contribution to the errors for the inelastic data at angles less than about 50°. The number of counts obtained in the inelastic peaks during the asymmetry runs was usually 500 or more, so that the fractional statistical error in the relative inelastic cross sections (N_L+N_R) was about 4% or less, depending on the amount of background or overlap. The statistical error in the asymmetry was typically $\Delta\epsilon\lesssim 0.12$. The peak-unfolding errors ΔN_0 and ΔN_B make similar contributions to the inelastic errors except at angles less than 50°, where they are largest. The counter efficiencies on each side of the beam are the same to within a 1% uncertainty in the solid angle defined by the collimator apertures. This uncertainty is negligible relative to the other contributions to ΔN.

The total fractional relative error $\pm\Delta\sigma/\sigma$ in the differential cross section at each angle is then $\pm\Delta N/N$, where ΔN is given by Eq. (2). Using Eq. (1), the errors propagate in the asymmetry measurements to produce an error $\pm\Delta\epsilon$ given by

$$\Delta\epsilon^2=\frac{1}{P_B^2}\left\{\left[\frac{2N_R\Delta N_L}{(N_L+N_R)^2}\right]^2+\left[\frac{2N_L\Delta N_R}{(N_L+N_R)^2}\right]^2\right\}, \tag{3}$$

where ΔN_L and ΔN_R are each given by Eq. (2).

Two other uncertainties are recognized but are not included in the relative error evaluated for each datum. Maximum beam-alignment uncertainties are estimated to be equivalent to a ±0.1° error in the average direction of the beam relative to the counters. The amount of spurious asymmetry this introduces depends on the actual asymmetry, the beam polarization, and the variation of the asymmetry and cross section with angle. We estimate a maximum misalignment error in the inelastic-asymmetry data of $\Delta\epsilon=0.03$. The other error is due to the over-all angular resolution, which was ±2.5° in the asymmetry runs and ±1° in the cross-section runs. These angular spreads correspond to an uncorrelated addition of the maximum divergence in the beam and of the angular acceptance of the counter collimators, including the effect of the finite size of the beam spot on the target. The effect of multiple scattering in the targets was negligible. The angular acceptance was adequate for the inelastic cross-section measurements, as could be verified by comparing the inelastic cross-section data obtained in the asymmetry runs to those obtained in the cross-section runs. The former, with 2.5 times the angular acceptance, agree excellently with the latter. The effect of the ±2.5° angular resolution on the inelastic-asymmetry measurements also appears to be minor. The oscillations observed in the inelastic asymmetries rise gently to maximum values near $\epsilon=+1$, and fall at a comparable rate to minima near $\epsilon=0$. It therefore seems that the only behavior of the inelastic asymmetries which could be obscured by the spread of ±2.5°

---

[20] D. F. Measday, Nucl. Instr. Methods 34, 353 (1965).

would be a rather unlikely, negative "spike" near the minima in their angular distributions.

C. Results

Tables of the inelastic asymmetry and cross-section data exist and will be sent upon request as long as the supply lasts. They may also be procured from the American Documentation Institute.[21] Plots of all of the data appear in the next section along with calculated curves. The error bars indicated in these plots denote the relative probable errors $\Delta\sigma$ and $\Delta\epsilon$ defined above.

The inelastic cross sections for iron and nickel have been measured[19] out to 90° for 40-MeV protons at Minnesota with an energy resolution comparable with the present measurements. Their agreement with the present data for the four transitions in ^{54}Fe is only fair. Our cross sections become increasingly higher than the previous values as the angle is reduced, and the discrepancies are larger for proton groups closer in energy to the elastic peak. However, the results do generally agree within their estimated uncertainties. In the previous work, the energy spectra were unfolded in a way which assumed a maximum contribution from the general background of unresolved, nearby peaks. Our method of unfolding the spectra involves more of an average of the maximum and minimum possible contributions, and this difference can account for the discrepancies in the ^{54}Fe data.

Our agreement with the previous Minnesota data for the two states in ^{58}Ni seems quite good except for the 1.45-MeV transition at angles smaller than 20°. There, the previous data are higher than the present results by almost a factor of 2. The opposite appears to be true of the inelastic cross section for ^{60}Ni, where our data for the first excited state are about a factor of 2 higher at the most forward angles. Elsewhere, the data for both transitions in ^{60}Ni are also in good agreement with previous values. These differences for the first excited states at small angles can be explained by systematic errors in either or both experiments in judging the contribution from the elastic peak.

The inelastic-asymmetry data extend over as large an angular region as the uncertainties in the measurement would allow. No meaningful asymmetry data could be obtained for the weaker 3^- state in ^{54}Fe at 4.8 MeV, for which the uncertainties in unfolding the energy spectra resulted in an intolerable probable error. The inelastic asymmetry results are shown in Fig. 3 along with *empirical* curves drawn through the data to illustrate our judgment of the trends. The curves for the 2^+ states in ^{54}Fe, ^{58}Ni, and ^{60}Ni are all identical and illustrate that, within present uncertainties, these asymmetries are very much alike. The same thing was done for the 3^- excitations in these nuclei. Agreement of the asymmetry results is particularly clear for the 2^+ states in ^{58}Ni and ^{60}Ni.

Inelastic asymmetries measured[14] with 18.6-MeV protons at Saclay have differed for some of the 2^+ excitations observed in isotopes of Ti, Cr, and Fe. There appeared to be two types, one of which was more similar to 16.5-MeV data[10] for 2^+ excitations in ^{60}Ni and ^{62}Ni. Most notably, a difference was detected between the asymmetries for the 1.41-MeV state in ^{54}Fe and the 2.97-MeV state in the same nucleus; the asymmetry for the lower-lying 2^+ state in ^{54}Fe was everywhere larger in algebraic value than that for the second 2^+ state, by as much as 0.3 at some angles. This amount is considered to be well outside any difference attributable to the Q values in a collective-model description. A close examination of our data in Fig. 3 in the light of the Saclay results does suggest that the maximum in the asymmetry near 70° for the 1.41-MeV state in ^{54}Fe may be shifted out in angle by about 5°, and may be 0.2 larger, than that for the other three iron and nickel results. But, clearly, this is not well established by our present data.

The differential cross sections for the two 2^+ excitations in ^{54}Fe seem similar in shape at 17.5 MeV,[22] 17.9 MeV,[23] and at 40 MeV (from this work and Ref. 19); however, at 18.6 MeV[2] the angular distribution measured for the 1.41-MeV state differs appreciably at larger angles from those observed for the first excited (2^+) states in ^{56}Fe, ^{58}Ni, ^{60}Ni, and ^{62}Ni. At 40 MeV the cross sections for both 2^+ states in ^{54}Fe are well described by assuming a one-phonon collective excitation. It would be interesting to see if more accurate asymmetry data for these two excitations in the 40-MeV energy region would reveal a difference not detected in the present inelastic cross-section measurements. On the collective model, the similarity in shape and magnitude of the cross sections for the two states in ^{54}Fe would suggest that they involve a considerable mixing of one- and two-phonon vibrations. Attributing a strong two-phonon component to the higher state, however, does not seem consistent with the Saclay measurements, since the data[14] for that state agree more closely with the data[10] for the first excited states in ^{60}Ni and ^{62}Ni. Combining our measurements with the Saclay results, the asymmetries for the first 2^+ states in ^{48}Ti, ^{56}Fe, ^{58}Ni, ^{60}Ni, and ^{62}Ni appear to agree with that for the second 2^+ in ^{54}Fe, while another kind of result is noticed for the first 2^+ states in ^{50}Ti, ^{52}Cr, and ^{54}Fe. It is noteworthy that the excitations in this second group might all involve a fairly pure $(1f_{7/2})^{\pm n}$ proton configuration and a closed neutron shell, while those in the first group are all more complicated.

Our result for the 2^+ excitation in ^{28}Si appears to

---

[21] Copies may be obtained by sending $1.75 for a microfilm copy and $2.50 for a photocopy to the American Documentation Institute Auxiliary Publication Project, Library of Congress, Washington, D. C. 20036. Deposited as Document Number *9613*.

[22] H. O. Funsten, N. R. Roberson, and E. Rost, Phys. Rev. **134**, B117 (1964).

[23] W. S. Gray, R. A. Kenefick, and J. J. Kraushaar, Nucl. Phys. **67**, 565 (1965).

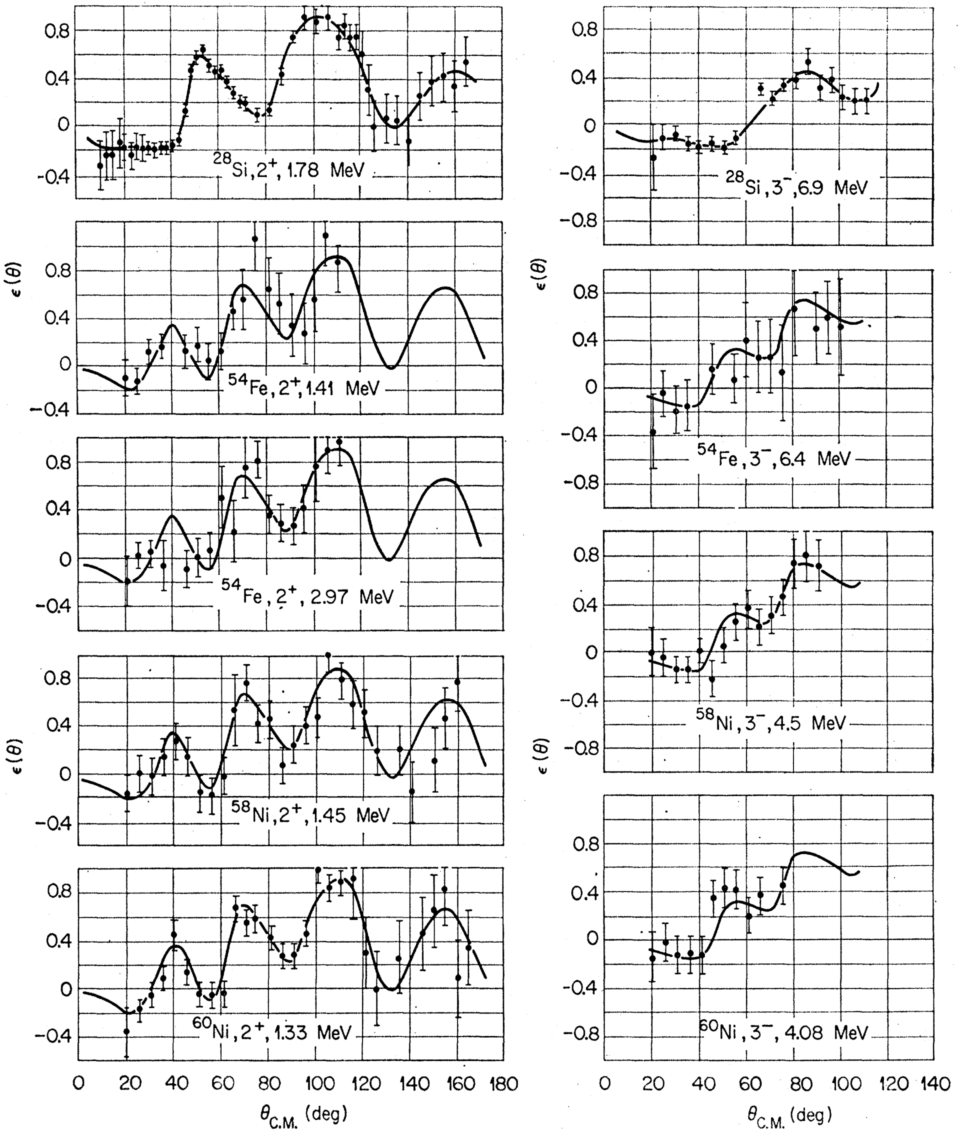

FIG. 3. Inelastic-asymmetry data. The curves shown are empirical and are identical for transitions in iron and nickel with the same multipolarity.

agree very well with the Birmingham measurements[12] at 30 and 50 MeV, assuming that the features of those data extrapolate to 40 MeV.

A prominent feature of all the 40-MeV inelastic asymmetries, for both 2^+ and 3^- excitations, consists of the large positive oscillations observed at the larger scattering angles, not unlike the general trend seen in elastic scattering. Also, all of the inelastic asymmetries appear to be negative at the most forward angles where their measurement was possible. These two characteristics of the data will be used frequently in evaluating the success of the collective-model analysis described in Sec. III.

III. ANALYSIS

A. Theory

The data were analyzed in the distorted-wave approximation assuming the collective-model generalization of the optical-model potential. The distorted-wave (DW) method for inelastic scattering upon entrance channel i to exit channel f is based upon the transition amplitude[6]

$$T_{i\to f}^{\rm DW}=\int d\mathbf{r}\,\Phi_f^{(-)*}(\mathbf{k}_f,\mathbf{r})\langle\psi_f|U|\psi_i\rangle\Phi_i^{(+)}(\mathbf{k}_i,\mathbf{r}). \qquad (4)$$

The distorted waves Φ for the relative motion of the projectile and target are generated by an optical-model potential $U_{\rm om}$ which is adjusted to reproduce the observed elastic scattering in each channel,

$$[\nabla^2+k^2-(2\mu/\hbar^2)U_{\rm om}(r)]\Phi(\mathbf{k},\mathbf{r})=0. \qquad (5)$$

The matrix element of the effective interaction U is taken between the internal states ψ of the target.

We assume a local, 11-parameter optical potential of the form

$$U_{\mathrm{om}}(r)=U_{\mathrm{Coul}}(r)-Vf(x)-i(W-4W_D d/dx')f(x') + (\hbar/m_\pi c)^2(V_S+iW_S)\boldsymbol{\sigma}\cdot\mathbf{l}(1/r)(d/dr)f(x_S)\,, \quad (6)$$

where the Woods-Saxon shape factors are $f(x_k)=(e^{x_k}+1)^{-1}$, $x_k=(r-r_kA^{1/3})/a_k$, for each of the "geometry" parameters $r_k=r_0,\ r_0',\ r_S;\ a_k=a,\ a',\ a_S$. $U_{\mathrm{Coul}}(r)$ is the Coulomb potential for a proton in the field of a uniformly charged sphere of radius $R_c=1.2A^{1/3}$ F and charge Ze. The optical potentials for the present elastic data were determined by searching simultaneously on both the cross-section and polarization measurements for each target. This search was accomplished with the computer program HUNTER[24] which attempts to find parameter values for Eq. (6) which minimize the quantity $(\chi_\sigma^2+\chi_P^2)$, where

$$\chi_\sigma^2=\sum_{i=1}^{N_\sigma}\{[\sigma_{\mathrm{expt}}(\theta_i)-\sigma_{\mathrm{theor}}(\theta_i)]/\Delta\sigma_{\mathrm{expt}}(\theta_i)\}^2\,,$$

and

$$\chi_P^2=\sum_{i=1}^{N_P}\{[P_{\mathrm{expt}}(\theta_i)-P_{\mathrm{theor}}(\theta_i)]/\Delta P_{\mathrm{expt}}(\theta_i)\}^2. \quad (7)$$

Here, $\sigma_{\mathrm{expt}}(\theta_i)$ and $P_{\mathrm{expt}}(\theta_i)$ are the data at angle θ_i, $\sigma_{\mathrm{theor}}(\theta_i)$ and $P_{\mathrm{theor}}(\theta_i)$ the calculated values, and $\Delta\sigma_{\mathrm{expt}}(\theta_i)$ and $\Delta P_{\mathrm{expt}}(\theta_i)$ the experimental uncertainties or weights, assigned to the measurements. Except where noted differently, the relative probable errors defined above were used to weight the elastic data.

In the DW calculations here, we do not modify the optical parameters used for the exit-channel distortion from those used for the entrance channel, i.e., from those which fit the elastic scattering data at the entrance-channel energy. Calculations have also been made in which the DW exit-channel parameters V, W, and W_D were changed according to the results of our previous study[9,25] of their energy dependence near 40 MeV: $dV/dE_p\simeq-0.22$, $dW/dE_p\simeq0.2$, $dW_D/dE_p\simeq-0.15$. This produced no appreciable difference from calculations which use the same parameters in both channels.

The inelastic interaction appropriate for exciting a 2^l-pole rotation or single-phonon surface oscillation of the target nucleus is obtained[5] by deforming the spherical optical potential (6). In the DW calculation, this interaction is taken to be the nonspherical part of the deformed potential which occurs to first order in the multipole deformation parameter β_l. For a given multipole, the strength of the resulting nuclear matrix element U_{fi}, and its dependence on the relative coordinate, are contained in a form factor $F(\mathbf{r})$. Originally, only the real, central terms in the optical potential were included, that is, allowed to contribute to the nonspherical interaction. In that case, one has the form factor $F(\mathbf{r})=f_{\mathrm{Re}}(\mathbf{r})+f_{\mathrm{CE}}(\mathbf{r})$, where $f_{\mathrm{Re}}(\mathbf{r})$ is the contribution from the nuclear term and $f_{\mathrm{CE}}(\mathbf{r})$ is that from the Coulomb term. The latter accounts for the possibility of Coulomb excitation, which has an amplitude adding coherently to the nuclear amplitude. These contributions to the total form factor are given[5] by

$$f_{\mathrm{Re}}(\mathbf{r})=(\beta_lR_0V/a_0)Y_{lm}(d/dx)f(x)\,, \quad (8)$$

and

$$f_{\mathrm{CE}}(\mathbf{r})=3\beta_l(2l+1)^{-1}Ze^2R_c{}^lY_{lm}r^{-l-1}\,,\quad \text{if } r\geq R_c\,,$$
$$=0\,,\quad \text{if } r<R_c. \quad (9)$$

The factors $R_0=r_0A^{1/3}$, $a_0=a$, V, and $f(x)$ are those appearing in Eq. (6) and are determined by fitting the elastic data. Calculations which include only the form factors (8) and (9) are termed "real coupling."

More recently, collective-model calculations have been carried out with "complex coupling," where both real and imaginary parts of the central portion of U_{om} are deformed. The imaginary part of the nonspherical interaction gives important contributions to the inelastic scattering of ^{3}He particles[8] and deuterons[26] and appears necessary to obtain reasonable values of β_l. Complex coupling results in a slight but consistent improvement in predictions of the shapes of the angular distributions for 2^+ and 3^- excitations for 40-MeV protons, but has a small ($\sim$10%) effect on β_l.[3] In complete analogy with the real form factor (8), the contribution from the imaginary, central terms in Eq. (6) is

$$f_{\mathrm{Im}}(\mathbf{r})=i(\beta_lR_0'W/a_0')Y_{lm}(d/dx')f(x') + i(\beta_lR_0'W_D/a_0')Y_{lm}(-4d/dx')(d/dx')f(x')\,, \quad (10)$$

where $R_0'=r_0'A^{1/3}$, $a_0'=a'$. The same deformation has been assumed for both real and imaginary parts of the optical potential.

In the present work, we also consider a contribution[16] from the spin-orbit term in Eq. (6). The spin-orbit form factor may also be written by analogy, noting that the factor $(Y_{lm}\boldsymbol{\sigma}\cdot\mathbf{l})$ is to be made Hermitian:

$$f_{\mathrm{so}}(\mathbf{r})=-(\beta_l{}^{\mathrm{so}}R_S/a_S)(V_S+iW_S)(\hbar/m_\pi c)^2 \times\tfrac{1}{2}(Y_{lm}\boldsymbol{\sigma}\cdot\mathbf{l}+\boldsymbol{\sigma}\cdot\mathbf{l}Y_{lm})(1/r)(d/dr)(d/dx_S)f(x_S). \quad (11)$$

We thus consider the form factor which results from deforming the complete potential, i.e., "complex-plus-spin-orbit coupling":

$$F(\mathbf{r})=f_{\mathrm{Re}}(\mathbf{r})+f_{\mathrm{CE}}(\mathbf{r})+f_{\mathrm{Im}}(\mathbf{r})+f_{\mathrm{so}}(\mathbf{r}). \quad (12)$$

The form taken here for the nonspherical $\boldsymbol{\sigma}\cdot\mathbf{l}$ interaction is to be tested phenomenologically by comparison with our data. It is perhaps the simplest such form but is by no means unique. In particular, if one casts the elastic interaction into the familiar Thomas form $\boldsymbol{\nabla}V_{\mathrm{so}}(r)\times\mathbf{v}\cdot\mathbf{S}$, then the spin-orbit term in the spherical

---

[24] R. M. Drisko (unpublished).

[25] B. J. Morton, R. H. Bassel, L. N. Blumberg, M. P. Fricke, E. E. Gross, A. van der Woude, and A. Zucker, Bull. Am. Phys. Soc. **11**, 13 (1966) and (to be published).

[26] J. K. Dickens, F. G. Perey, and G. R. Satchler, Nucl. Phys. **73**, 529 (1965).

optical potential (6) is equivalent to the expression

$$U_{\mathrm{so}}(r)=[2\mu/(m_\pi c)^2]\nabla[(V_S+iW_S)f(x_S)]\times\mathbf{v}\cdot\mathbf{S}. \quad (13)$$

But if the deformation is introduced into $f(x_S)$ at this point, there are in addition to the term (11) some other contributions to the form factor which arise from the nonradial components of the gradient operator in the above expression. These contributions are very complicated,[27] and at this stage it is considered reasonable to explore the simpler form factor (11). We do, however, allow the strength β_l^{so} of the spin-orbit interaction to differ from the strength β_l of the central interaction. If $\beta_l^{\mathrm{so}}=\beta_l$, then in the DW approximation the inelastic cross section is simply proportional to β_l^2, and the asymmetry is independent of β_l. For $\beta_l^{\mathrm{so}}\neq\beta_l$, the shapes of the calculated cross sections and asymmetries depend upon the ratio $(\beta_l^{\mathrm{so}}/\beta_l)$.

In the collective-model interaction, with or without a deformed spin-orbit potential, the operator which affects the target nucleus coordinates is of rank l, so that the total angular momentum j transferred to the nucleus is equal to l, the multipole order.[6] The parity change is $\Delta\pi=(-)^l$, so that only normal parity transitions are allowed in first order. The collective operator is usually thought of as spatial only, and not to affect the spins of the target nucleons, so that in this sense the "spin transfer" may be regarded as zero, $s=0$. The *projectile* proton may undergo spin-flip both under the influence of the $\boldsymbol{\sigma}\cdot\mathbf{l}$ coupling in the elastic distortion, and of the deformed $\boldsymbol{\sigma}\cdot\mathbf{l}$ term if this is included. The latter term induces inelastic transitions which for the projectile may be called $s'=1$. Thus the algebra of the angular-momentum transfer (in which we may have $s\neq s'$) becomes a little more complicated than that usually encountered. A similar situation arises in a "microscopic" description of inelastic scattering when two-body spin-orbit or tensor forces are included (see Sec. IIID, and also Appendix 2 of Ref. 34). A trial calculation for the 2^+ state of ^{60}Ni was made with $l=j=2$ but simply adding a 20% admixture of $s=1$ with the same form factor (12) as $s=0$; the asymmetry and cross section produced differed very little from those with $s=0$ alone. All the calculations discussed below were made with $s=0$.

B. Exploratory Calculations

To examine the effects of the form factors in the prediction of inelastic asymmetry, a number of calculations[28] was first made for the targets ^{28}Si and ^{60}Ni. The findings were the same for the two nuclei and will be illustrated only for ^{60}Ni.

Different sets of optical-model parameters, all of which gave fairly good fits to the elastic cross-section data out to large angles, were used in these calculations. Regardless of the contributions [Eqs. (8) to (11)] included in the form factor $F(\mathbf{r})$, a good fit to the inelastic asymmetry data for the 2^+ excitation was not obtained unless the potential also gave a good fit to the elastic polarization data out to large angles. The goodness of fit to the inelastic asymmetry was much more strongly correlated to the quality of fit to the elastic polarization than to the elastic cross section. This correlation seems consistent with the theory of Austern and Blair,[29] in which the elastic and inelastic scattering amplitudes are simply related.

Typical results are illustrated in Fig. 4, using the two sets of optical parameters given in Table I. The "best cross-section" parameters are the "best-fit" results from Ref. 9, which were deduced from the elastic data by minimizing $(\chi_\sigma^2+\chi_P^2)$. The "best polarization" parameters were deduced from the same data, but with greater weights, i.e., smaller errors, ΔP_{expt}, assigned to the large-angle polarization data. The calculations of inelastic scattering illustrated in Fig. 4 include all the contributions to the total form factor, with $\beta_2=0.22$ and $\beta_2^{\mathrm{so}}=1.5\beta_2$.

1. *Form Factors*

The effects of the form factors in the calculation of the inelastic scattering from ^{60}Ni are shown in Fig. 5 for the 2^+ excitation and in Fig. 6 for the 3^- excitation. This is illustrated for the best polarization potential of Table I, and again we use $\beta_l^{\mathrm{so}}=1.5\,\beta_l$ with $\beta_2=0.22$ and $\beta_3=0.18$. For both the asymmetries and cross sections, the dotted curves are for real coupling only, $F(\mathbf{r})=f_{\mathrm{Re}}(\mathbf{r})+f_{\mathrm{CE}}(\mathbf{r})$. This calculation fails to reproduce the oscillations observed in both the asymmetry and cross section for the 2^+ transition. The Coulomb form factor has a very small effect. Calculations for this excitation which do not include $f_{\mathrm{CE}}(\mathbf{r})$ differ from those which do by about 10% in the cross section at most angles and by an amount less than 0.05 in the asymmetry. The difference is smaller for 3^- excitations. The curves with short dashes in Figs. 5 and 6 were calculated by adding the spin-orbit form factor to the real form factor, $F(\mathbf{r})=f_{\mathrm{Re}}(\mathbf{r})+f_{\mathrm{CE}}(\mathbf{r})+f_{\mathrm{so}}(\mathbf{r})$. This increases the absolute value of the asymmetry but still fails to reproduce the oscillations in the 2^+ data. The curves with dots and dashes are for complex coupling, $F(\mathbf{r})=f_{\mathrm{Re}}(\mathbf{r})+f_{\mathrm{CE}}(\mathbf{r})+f_{\mathrm{Im}}(\mathbf{r})$. The oscillations are now larger, but the agreement with the data is not good. The asymmetry is not positive enough, and the oscillations in the cross section seem too large. Finally, all the terms are included for the form factor of Eq. (12), which

---

[27] R. M. Drisko (private communication).

[28] The inelastic-scattering calculations were made, with a slightly amended version of the code JULIE, by R. M. Drisko (unpublished), with which it is possible to calculate a scattering amplitude for the spin-orbit form factor (11) and add it coherently to the other amplitudes, which are calculated conventionally. This version of the code differs from the code SALLY described in Ref. 5 by this feature and by the inclusion of the spin-orbit term in the distorting potential (as discussed in Ref. 6).

[29] N. Austern and J. S. Blair, Ann. Physics (N. Y.) 33, 15 (1965).

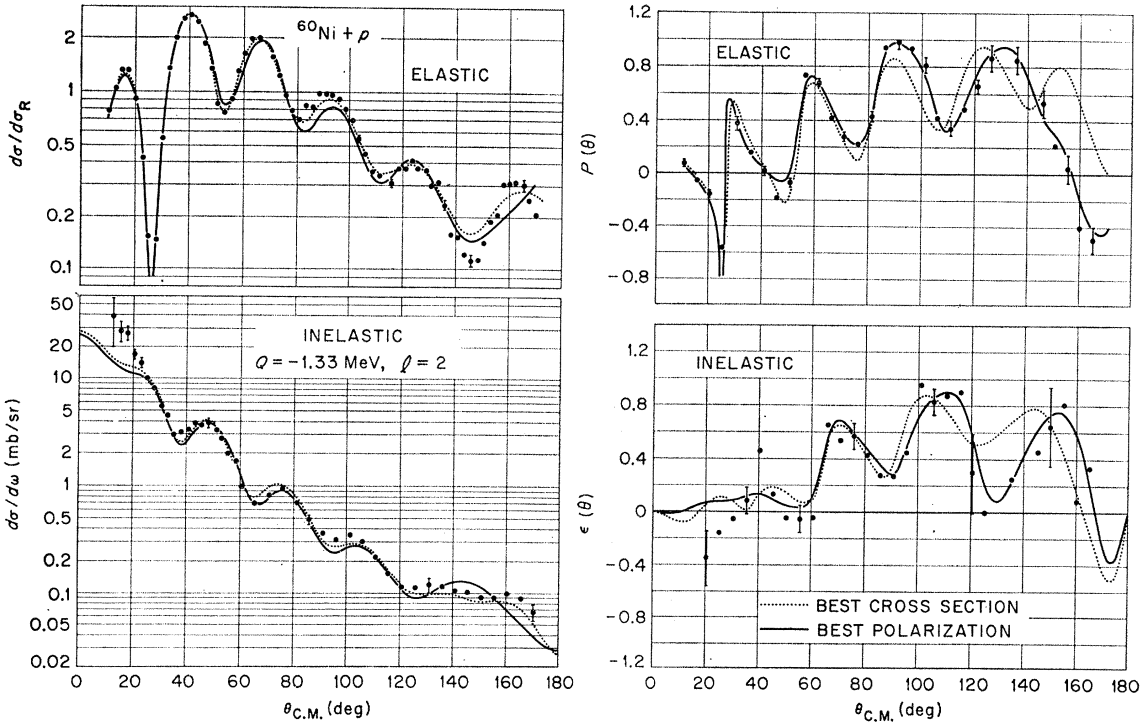

FIG. 4. Correlation in fits to elastic and inelastic data; DW calculations are shown for the quadrupole excitation in ^{60}Ni. The two calculations use the two sets of optical-model parameters given in Table I, which produce the elastic fits also shown in the figure.

produces the solid curves in these figures and the best agreement with our data.

For all of the optical potentials tried for ^{28}Si and ^{60}Ni, the large positive oscillations observed at large angles in the asymmetry data for the 2^+ excitations appear in the calculations only if the imaginary form factor is included. In the calculations of both 2^+ and 3^- asymmetries, the contribution $f_{\mathrm{Im}}(\mathbf{r})$ tends to increase the magnitude of the oscillations, while $f_{\mathrm{so}}(\mathbf{r})$ both increases the oscillations and shifts the curve to more positive values. Collective-model calculations of 2^+ asymmetries using only real coupling have been made by Perey[15] for the Saclay Ni data[10] and by Greenlees[12] for the Birmingham ^{12}C and ^{28}Si data. These also fail to reproduce the large positive oscillations observed at large angles.

The 40-MeV asymmetry data at forward angles, smaller than about 50° for ^{60}Ni, are not reproduced by deforming the complete potential in the present treatment. Indeed, our calculations for the 2^+ state in ^{28}Si which do not include the spin-orbit form factor appear slightly better at small angles since they tend to be more negative, like the data. This forward-angle discrepancy will be shown to be quite a general result when the calculations are presented for the rest of our inelastic data. The cross-section calculation for the 2^+ state in ^{60}Ni also appears to be too low at the most forward angles, although this is not generally true for the other 2^+ excitations we measure.

The ratio $\beta_l^{\mathrm{so}}/\beta_l$ of the spin-orbit deformation to the central deformation has been taken to be 1.5 for these and the rest of our calculations, although this choice is somewhat arbitrary. The effect of varying the strength of the spin-orbit form factor is illustrated in Fig. 7 for the 2^+ calculation, using the best polarization potential of Table I and the complete form factor (12). A slight but consistent preference for a value of β_l^{so} about one to two times that of β_l has been noticed for both the 2^+ cross sections and asymmetries at larger angles. As indicated in Eq. (11), both real and imaginary parts of the spin-orbit potential are deformed with the same strength β_l^{so}. However, since all of our results for the

TABLE I. Optical-model parameters for ^{60}Ni which produce fits to elastic data shown in Fig. 4. The "best cross-section" parameters are the "best-fit" values of Ref. 9.

Potential	V (MeV)	W (MeV)	W_D (MeV)	V_S (MeV)	W_S (MeV)	r_0 (F)	a (F)	r_0' (F)	a' (F)	r_S (F)	a_S (F)
Best cross section	48.3	5.4	1.6	7.0	0	1.12	0.77	1.47	0.60	0.98	0.86
Best polarization	52.9	5.5	2.8	4.7	−0.7	1.06	0.87	1.41	0.49	1.04	0.52

optical potential have $|W_S| \ll V_S$, calculations which include the imaginary part of the spin-orbit form factor differ very little from those which do not.

Some investigation was made of the effect on the inelastic asymmetry calculation of varying the spin-orbit geometry parameters from their best polarization values of Table I. The 2^+ calculation for ^{60}Ni was made for values of these parameters in the range $1.0\ \text{F} \leq r_S \leq 1.2\ \text{F}$ and $0.5\ \text{F} \leq a_S \leq 0.7\ \text{F}$. The rest of the optical parameters were not readjusted; the fit to the elastic data was not preserved. These changes were made separately (i) in only the form factor $f_{\text{so}}(\mathbf{r})$; (ii) in only the elastic distortion, i.e., in the optical potential used to generate the distorted waves; and (iii) in both the form factor and the distortion. For each change the four types of form factor of Fig. 5 were used. This produced no difference in the general features of the asymmetry curves in Fig. 5. Their relative degree of positiveness and amount of oscillation remained unchanged, and in no case was the predicted asymmetry negative at the most forward angles.

In an attempt to judge further the importance of the imaginary form factor $f_{\text{Im}}(\mathbf{r})$, we have tried to reproduce the observed asymmetry with calculations in which this form factor is left out and the real form factor $f_{\text{Re}}(\mathbf{r})$ is varied. The distortion was still determined by the fit to the elastic scattering, but the real form factor was no longer given by its collective model

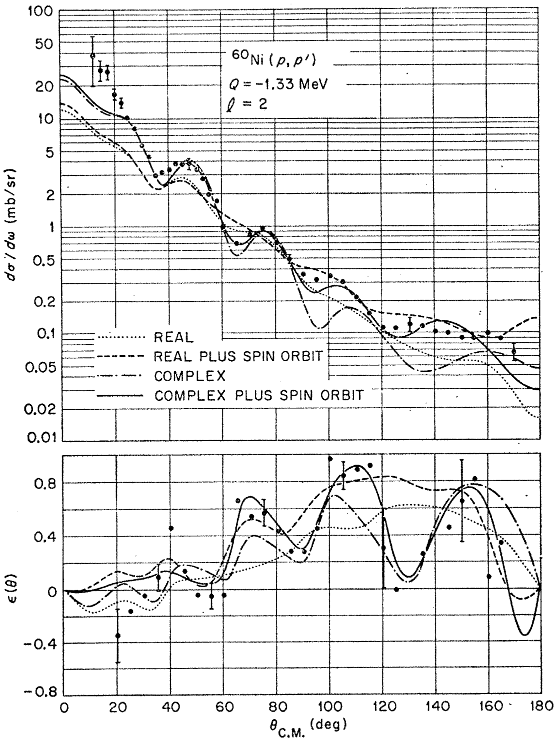

FIG. 5. Effects of form-factor options for quadrupole transition; DW calculations for ^{60}Ni are shown which include different contributions to the form factor, as described in the text.

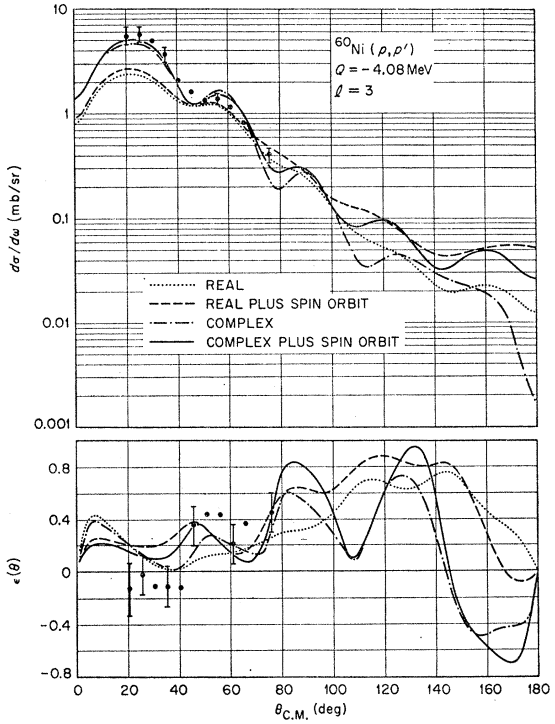

FIG. 6. Effects of form-factor options for octupole transition. The calculations of Fig. 5 are repeated for the 3^- state in ^{60}Ni.

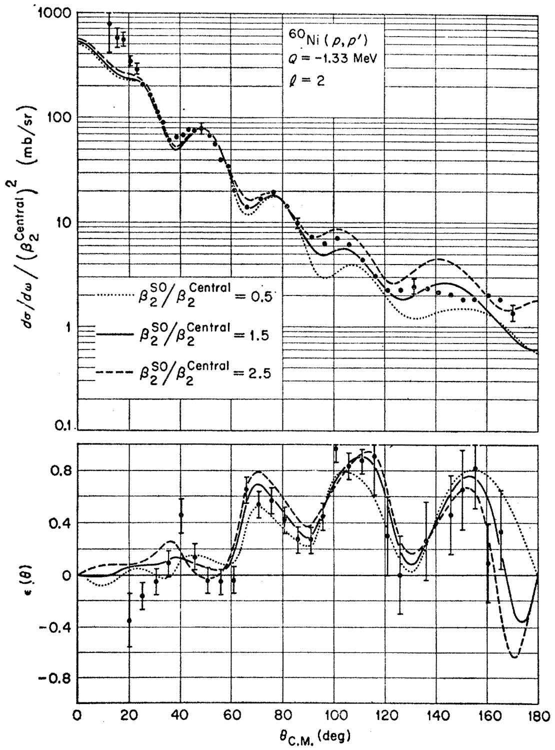

FIG. 7. Relative strength of spin-orbit form factor; DW calculations are shown for the quadrupole excitation in ^{60}Ni which use different ratios of the deformation parameters for the spin-orbit and central parts of the optical potential. The cross-section data are plotted for $\beta_2^{\text{cent}} = 0.22$.

prescription. In doing this, we used the shape of the collective model form factor (8) but varied its width and radial position by changing the parameters R_0 and a_0 from their collective-model values $r_0A^{1/3}$ and a, i.e., from the values used for the distorted waves. The calculations were carried out for the 2^+ state in ^{60}Ni with the distortion given by the best polarization potential of Table I. At each of the values $R_0=0.7$, 1.0, and 1.3 times the collective-model radius ($r_0A^{1/3}$), calculations were made for $a_0=0.5$, 0.8, 1.0, 1.2, and 1.5 times the collective-model diffusivity a. For each of these, the calculation was made with and without including the spin-orbit contribution $f_{\text{so}}(\mathbf{r})$. The result was that for any of the radii R_0, and with or without a spin-orbit contribution $f_{\text{so}}(\mathbf{r})$, large oscillations in the inelastic asymmetry were produced only with the most sharply peaked form factor having a diffusivity parameter a_0 of 0.5 times the collective-model value $a=0.87$. But with this diffusivity, the asymmetry data were still not reproduced. For $R_0=0.7r_0A^{1/3}$ and $a_0=0.5a$, the asymmetry calculation was negative at larger angles, with or without a contribution $f_{\text{so}}(\mathbf{r})$. For $R_0=1.0r_0A^{1/3}$ and $a_0=0.5a$, the asymmetry became positive, but the oscillations were almost exactly out of phase with the data. For $R_0=1.3r_0A^{1/3}$ and $a_0=0.5a$, the angular interval between oscillations was much less than that observed. The inelastic cross section was poorly reproduced in every case, although the disagreement was less pronounced than that for the asymmetry. Except for the collective-model values of R_0 and a_0, the main disagreement with the shape of the cross-section data was a difference in phase of up to $\pm10°$ in the forward hemisphere. We conclude that within the limits of this study, the contribution $f_{\text{Im}}(\mathbf{r})$ is essential in reproducing the oscillations observed at larger angles in the inelastic asymmetry for this 2^+ excitation.

The calculations of inelastic asymmetry ϵ are very nearly identical to calculations of the inelastic polarization P made in the same way. While the difference $P-\epsilon$ varies considerably with the form-factor options of Fig. 5, and increases with the magnitude of Q, it was in no case very large. In the calculations for the 2^+ excitations in iron and nickel, we find $0\lesssim(P-\epsilon)\lesssim0.005$ at forward angles and $0\lesssim(P-\epsilon)\lesssim0.01$ at back angles. For the 3^- states the difference is larger and usually of the opposite sign: $0\lesssim(\epsilon-P)\lesssim0.05$ at forward angles and $0\lesssim(\epsilon-P)\lesssim0.1$ at back angles. The probability of spin-flip is sensitive to the form factor used, as is indicated by the variation of $P-\epsilon$ with the form factor options of Fig. 5. Angular-correlation measurements which isolate the spin flip amplitudes[30] would provide another sensitive test of the deformed spin-orbit interaction and also of the possible presence of $s=1$ admixtures in normal parity excitations.

2. *Distorted-Wave Method and Coupled Equations*

The DW calculation was compared to a two-channel coupled-equations[31] calculation including the ground state and the 2^+ state of ^{60}Ni. The latter treats the coupling between the two states exactly, as opposed to the first-order treatment of the DW method. To make use of the options readily available in the coupled equations computer program[32] at this laboratory, a complex coupling calculation of the inelastic polarization (not the asymmetry) was made which did not include the Coulomb excitation amplitude. Also, a form of the optical potential was used in which the values of the spin-orbit geometry parameters r_S and a_S are taken equal to the values r_0 and a of the real central term, and the spin-orbit term is taken to be real, $W_S=0$. The solid curves in Fig. 8 are the elastic and inelastic predictions using a coupling strength of $\beta_2=0.22$ and the best polarization parameters of Table I, with the changes $r_S=1.06$ F, $a_S=0.87$ F, and $W_S=0$.

To compare these calculations to our DW treatment, we must first obtain new optical-model parameters which, in a one-channel calculation, give the same elastic scattering as the coupled-equations calculation. The dashed curves in Fig. 8 for the elastic cross section and polarization were produced by searching on the elastic coupled-equations predictions out to 120° with the code HUNTER. Only the parameters W and W_D were varied from the values used in the coupled-equations calculation; the fits could presumably be improved if all the parameters were varied. One expects the absorp-

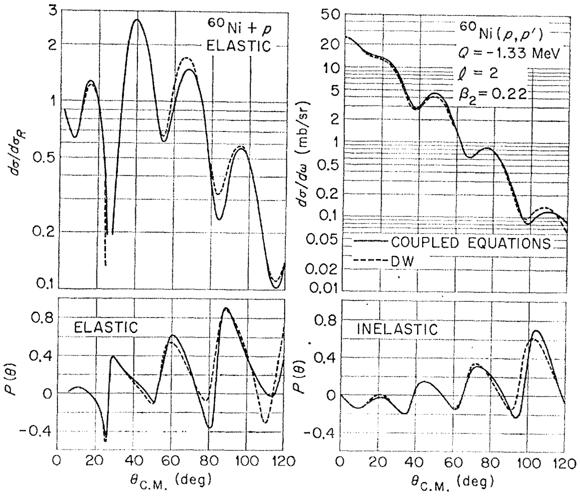

FIG. 8. Comparison to coupled-equations calculation. The solid curves are two-channel, coupled-equations predictions of elastic and inelastic scattering using the parameters given in the text. The dashed curves for elastic scattering are one-channel fits to the coupled-equations results, produced by varying only the parameters W and W_D. The dashed curves for inelastic scattering are DW calculations using the modified parameters.

---

[30] See, e.g., Ref. 15. For a $0^+\rightarrow2^+\rightarrow0^+$ transition, only $m_j=\pm1$ contribute when the γ detector is normal to the scattering plane.

[31] See, e.g., T. Tamura, Rev. Mod. Phys. **37**, 679 (1965).

[32] These calculations were made with the coupled-equations code of T. Tamura (unpublished).

tion to be somewhat larger in the one-channel calculation of elastic scattering, to compensate for the flux lost to the 2^+ excitation. The new values found were $W=6.55$ MeV and $W_D=2.25$ MeV. Thus, W increased by 20% from the coupled-equations value, but W_D decreased 20%; the sum $W+W_D$ increased only 6.4%. The dashed curves in Fig. 8 for the inelastic cross section and polarization are DW results using the optical parameters with these "corrected" absorptive strengths. One-channel calculations were also made using the same (uncorrected) parameters as in the coupled-equations method, and the results for both the elastic and inelastic scattering were nearly identical to those obtained with the modified values of W and W_D. The DW fits to the coupled-equations results for the inelastic scattering are seen to be at least as good as the agreement produced for the elastic scattering. We therefore conclude that the DW approximation is adequate for the present data, inasmuch as the higher-order effects included in the two-channel calculation are small.

C. Optical-Model Parameters

After the exploratory studies of ^{28}Si and ^{60}Ni, calculations were carried out for all of our data in a systematic fashion. The first task was to find optical-model parameters for the four targets which would give optimum fits to the elastic-polarization data while sacrificing the fits to the elastic cross-section data as little as possible. The polarization data for ^{28}Si, ^{58}Ni, and ^{60}Ni are more extensive, and calculations were first made for these targets with errors ΔP_{expt} assigned at large angles which were smaller than the experimental uncertainties. Using the results of these calculations as starting values for the parameters, with the ^{54}Fe potential taken equal to that found for ^{58}Ni, searches were made for the four targets using exclusively the experimental uncertainties to weight $\chi_\sigma^2+\chi_P^2$. However, the "final" parameter values were taken at that point when the search routine would start to sacrifice the fit to the general trend of the back-angle polarization data in order to achieve a slight improvement in $\chi_\sigma^2+\chi_P^2$, as happened for all three targets ^{28}Si, ^{58}Ni, and ^{60}Ni. In this way we have emphasized the elastic-polarization data to some extent, and the optical-model parameters thus found are somewhat different from those deduced in a previous analysis[9] of these same data, one which relied more strongly on the $\chi_\sigma^2+\chi_P^2$ criterion using the experimental uncertainties for ΔP_{expt}.

The resultant fits to the elastic data are shown in Fig. 9; and the optical parameters, predicted reaction cross sections σ_R, and values of χ^2/N are listed in Table II. The χ^2 values correspond to the experimental uncertainties. The results were not entirely successful for ^{28}Si and ^{54}Fe, while fairly good fits to the data were obtained for ^{58}Ni and ^{60}Ni. Subjectively, the present fits to the cross-section data appear very similar in quality to those of Ref. 9. For ^{54}Fe, the previous cross-section fit is slightly better near 90°; for ^{60}Ni the present fit is slightly better near 90°; and for ^{28}Si and ^{58}Ni the fits are very much alike. The fits to the polarization data for ^{54}Fe are also quite similar, but the present potentials somewhat improve the agreement with the large-angle polarizations for ^{28}Si, ^{58}Ni, and ^{60}Ni, without sacrificing the fit at forward angles. For ^{28}Si, the previous calculation of the polarization is 20° out of phase with the data at 110°, while the present calculation is a little closer. For ^{58}Ni and ^{60}Ni, the previous calculation (see Fig. 4) gave an extra oscillation near 140° which is not observed in the data, and which is eliminated in the present calculations. The present value of $\chi_\sigma^2+\chi_P^2$ is 20% worse for ^{28}Si, 5% worse for ^{54}Fe, 10% better for ^{58}Ni, and 35% better for ^{60}Ni. The predicted reaction cross section for each target is the same as the previous value to within 1% for three of the targets and differs by 2% for ^{60}Ni.

The values of the spin-orbit geometry parameters r_S and a_S vary considerably from target to target and also between the previous and present results. In the process of obtaining the present fits, however, it was observed that a rather wide range of these parameter values produce reasonable fits. For ^{60}Ni, changing r_S from 1.05 to 1.00 F and a_S from 0.5 to 0.7 F, together with very minor changes in the rest of the parameters, gave somewhat better fits to the cross section with only a slight sacrifice of the polarization fit. In going from $r_S=1.00$ F to $r_S=0.975$ F, and from $a_S=0.7$ F to $a_S=0.8$ F, the last "bump" in the cross section at 160° begins to come into better agreement at the expense of the polarization at the same angle. For values of a_S greater than 0.80 F, the polarization fit becomes much worse while the cross-section fit is only slightly improved. This tendency of the polarization data to favor

TABLE II. 40-MeV optical-model parameters which produce fits to elastic data shown in Fig. 9.

Nucleus	V (MeV)	W (MeV)	W_D (MeV)	V_S (MeV)	W_S (MeV)	r_0 (F)	a (F)	r_0' (F)	a' (F)	r_S (F)	a_S (F)	$\frac{\chi_\sigma^2}{N_\sigma}$	$\frac{\chi_P^2}{N_P}$	σ_R (mb)
^{28}Si	44.61	1.39	4.41	5.84	−0.36	1.134	0.733	1.409	0.537	1.012	0.632	30.1	13.5	645
^{54}Fe	47.61	5.06	0.12	4.41	−0.61	1.104	0.800	1.587	0.583	1.045	0.659	7.9	20.8	998
^{58}Ni	51.11	5.71	0.74	5.19	−0.24	1.080	0.798	1.531	0.430	1.043	0.614	6.3	21.1	1019
^{60}Ni	51.59	4.70	3.55	7.03	−0.77	1.081	0.815	1.410	0.525	0.975	0.789	8.0	8.1	1104

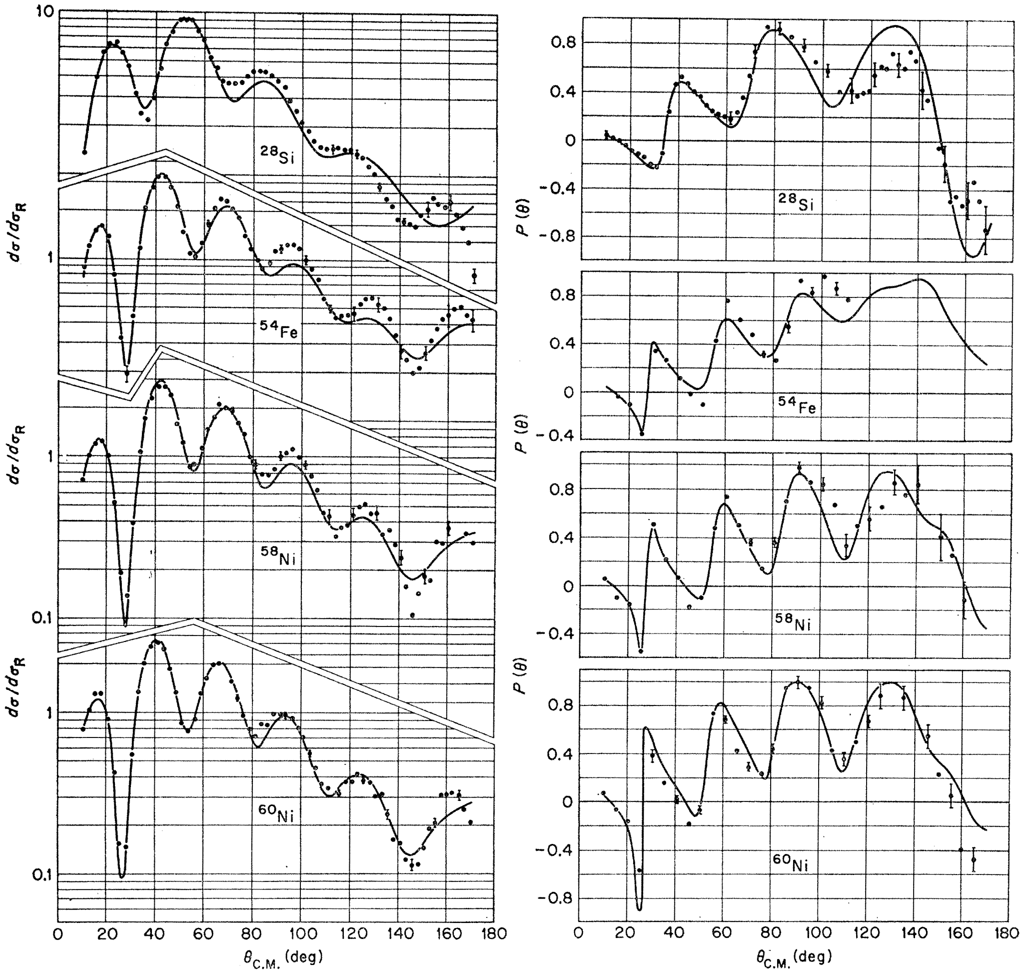

FIG. 9. Elastic cross-section and polarization data and their optical-model fits using parameters of Table II.

smaller values of a_S has also been found in an analysis[33] of 30-MeV proton data. The present results have smaller values of both r_S and a_S than the previous results for these data. Both results give values for r_S which are consistently smaller than those for the real radius r_0. The present values have an average of $r_0 - r_S$ equal to 0.08 F, as compared with the previous[9] average for 11 targets of 0.10 F, and the previous average for the four targets investigated here of 0.07 F.

The parameters r_0' and a' in Table II also vary considerably from target to target, but in a way consistent with previous findings for the imaginary potential. It has been observed[3] that the differential cross sections for 40-MeV protons can be fitted equivalently out to fairly large angles by imaginary potentials which may differ in the nuclear interior but which are similar in their "tails", say, for $r \gtrsim r_0 A^{1/3}$. To produce a tail with a volume potential ($W \gg W_D$) which is similar to that for a surface form ($W \ll W_D$), the volume potential must have a radius parameter r_0' which is larger than that for the surface potential. This is consistent with the values of Table II in that ^{54}Fe and ^{58}Ni have $r_0' \simeq 1.55$ F and $W \gg W_D$, while ^{28}Si and ^{60}Ni have $r_0' \simeq 1.41$ F and more comparable values of W and W_D.

The greatest difference between the previous[9] and present 40-MeV potentials is believed to be in the geometry parameters found for the real, central well. For each of the three targets with large-angle polarization data, a significant improvement in the fits to those data always occurred at a point in the automatic searching procedure when the radius parameter r_0 became smaller and the diffusivity a became larger. When compared with the previous values, the new results show a consistent decrease of 0.03–0.04 F in the value of r_0 for ^{28}Si, ^{58}Ni, and ^{60}Ni, and an increase of 0.02–0.04 F in the value of a. While this is only a change of some 4% in the parameter values, the preference of the polarization data for the new values seems quite strong. However, better large-angle polarization data and more extensive analysis will be necessary at 40 MeV to establish confidently the values of these parameters to such an accuracy. We note also that the radius parameter r_0 seems to be smaller for the Ni isotopes

---

[33] G. R. Satchler, Nucl. Phys. A92, 273 (1967).

than for the other targets, both in the present work and in the previous analysis of the data for 11 targets.

D. Predictions of Inelastic Scattering

Using the potentials of Table II, we have carried out DW calculations for all of the inelastic transitions. Each of the form-factor options, real and complex coupling, with and without $f_{\rm so}(\mathbf{r})$, was used again for every excitation, with the same results as those illustrated in Fig. 5 and Fig. 6. The new results are not repetitious since different optical parameters are involved. In particular, the potential for ^{58}Ni has almost pure volume absorption ($W=7.7\ W_D$), while that for ^{60}Ni is more evenly mixed ($W=1.3\ W_D$). Yet the DW calculations, including those with a contribution $f_{\rm Im}(\mathbf{r})$ to the total form factor, are almost identical. It has been verified by calculation, however, that the inelastic asymmetry is fairly sensitive to *arbitrary* changes in the strength or shape parameters of the imaginary form factor $f_{\rm Im}(\mathbf{r})$. By plotting the radial dependence of each of the form factors derived from the optical parameters of Table II, it has been observed that the form factors for ^{58}Ni agree very closely with those for ^{60}Ni in their tails, $r\gtrsim 6$ F. However, the form factors $f_{\rm Im}(\mathbf{r})$ and $f_{\rm so}(\mathbf{r})$, which contain the second derivative of the Woods-Saxon potential, are quite different for the two targets in the nuclear interior, say, $r\lesssim 5$ F. The same is true for the radial shapes of the imaginary and spin-orbit terms in the optical potential, in that the terms for ^{58}Ni and ^{60}Ni agree well only in their tails. Although the imaginary term in the optical potential for 40-MeV protons is consistent[9] with a mean free path in nuclear matter of about 7 F, it would nevertheless appear that our calculations of elastic and inelastic scattering are fairly insensitive to contributions from the nuclear interior.

Distorted-wave calculations of inelastic cross sections which use the complete form factor (12), with $(\beta_l^{\rm so}/\beta_l)=1.5$, and the potentials of Table II are compared with the data in Fig. 10. The values of the central-well deformation parameter β_l deduced from adjusting the normalization of the calculations to match the data are given in the figure. These are in good agreement with those found[3] from the previous Minnesota data.[19] The largest discrepancy (30%) occurs for the 1.41- and 4.8-MeV states in ^{54}Fe, and is mostly due to the experimental discrepancy noted in Sec. II. The deformation parameters for the states in ^{58}Ni and ^{60}Ni agree with those found in Ref. 3 to within 5%. As can be seen, the shape of the cross sections for the heavier nuclei is predicted rather well out to very large angles. The exceptions to this are the anomalous bump observed near 100° in the cross section for the 2^+ state in ^{58}Ni and the data at angles smaller than 20° for the 2^+ state in ^{60}Ni. The latter could be due to a systematic error in reducing the data, as discussed in Sec. II, but the former appears to be real. The predictions for the states in ^{28}Si are poor, but little else can be said until a more successful fit is achieved to the elastic data for that target. The deformation parameters indicated for the ^{28}Si data are tentative at best. The prediction for the 6.9-MeV level observed in ^{28}Si is very bad and does not confidently identify the multipole order.

The inelastic-asymmetry data and their DW predictions are shown in Fig. 11. The calculations are the same as those shown for the cross sections in Fig. 10. As was the case in the exploratory calculations for ^{28}Si and ^{60}Ni, the present form of the theory appears to give a good account of the large oscillations observed at large angles, but does not appear to reproduce the data at angles smaller than about 50° for iron and nickel and smaller than 70° for silicon. The calculations using the complete form factor were invariably positive at small angles, while the data for both 2^+ and 3^- excitations appear to be negative. The calculations for the two 2^+ states in ^{54}Fe do not seem to oscillate enough to reproduce the minima observed near 90°. This is reminiscent of the situation for the good cross section potential of Fig. 4 and leads one to suspect that the unmeasured, large-angle elastic polarization would not agree well with the optical-model curve in Fig. 9.

IV. CONCLUSIONS

The sensitivity of the inelastic-asymmetry calculation is leading to refinements in the collective-model interaction investigated for the present data. The fact that the calculation requires a very careful treatment of the elastic distortion adds to the credibility of the DW-method. Based on this experinece, future inelastic asymmetry or polarization measurements should provide valuable contributions to our understanding of the inelastic scattering of medium-energy protons.

Measurement of the elastic and inelastic scattering at large angles has proved an essential part of this work. The elastic-polarization data at large angles demand new values of the optical-model parameters, and these produce a significant improvement in the predictions of inelastic asymmetry. At present it appears that more back-angle elastic-polarization data will be necessary to establish the optimum parameter values for 40-MeV protons, or to decide whether or not the present form of the potential can in fact account simultaneously for the elastic cross section and polarization at all angles.

The intensity and polarization of our proton beam, and the over-all energy resolution we achieved, were marginal for the excitations measured. To extend this study to weaker transitions, considerably better resolution would be necessary. Polarized proton sources for linear accelerators and cyclotrons, together with solid-state detectors or magnetic analysis of the scattered protons, afford exciting opportunities to explore excitations amenable to a more microscopic description of the effective interaction and nuclear wave functions.[34] As

---

[34] See, e.g., G. R. Satchler, Nucl. Phys. 77, 481 (1966).

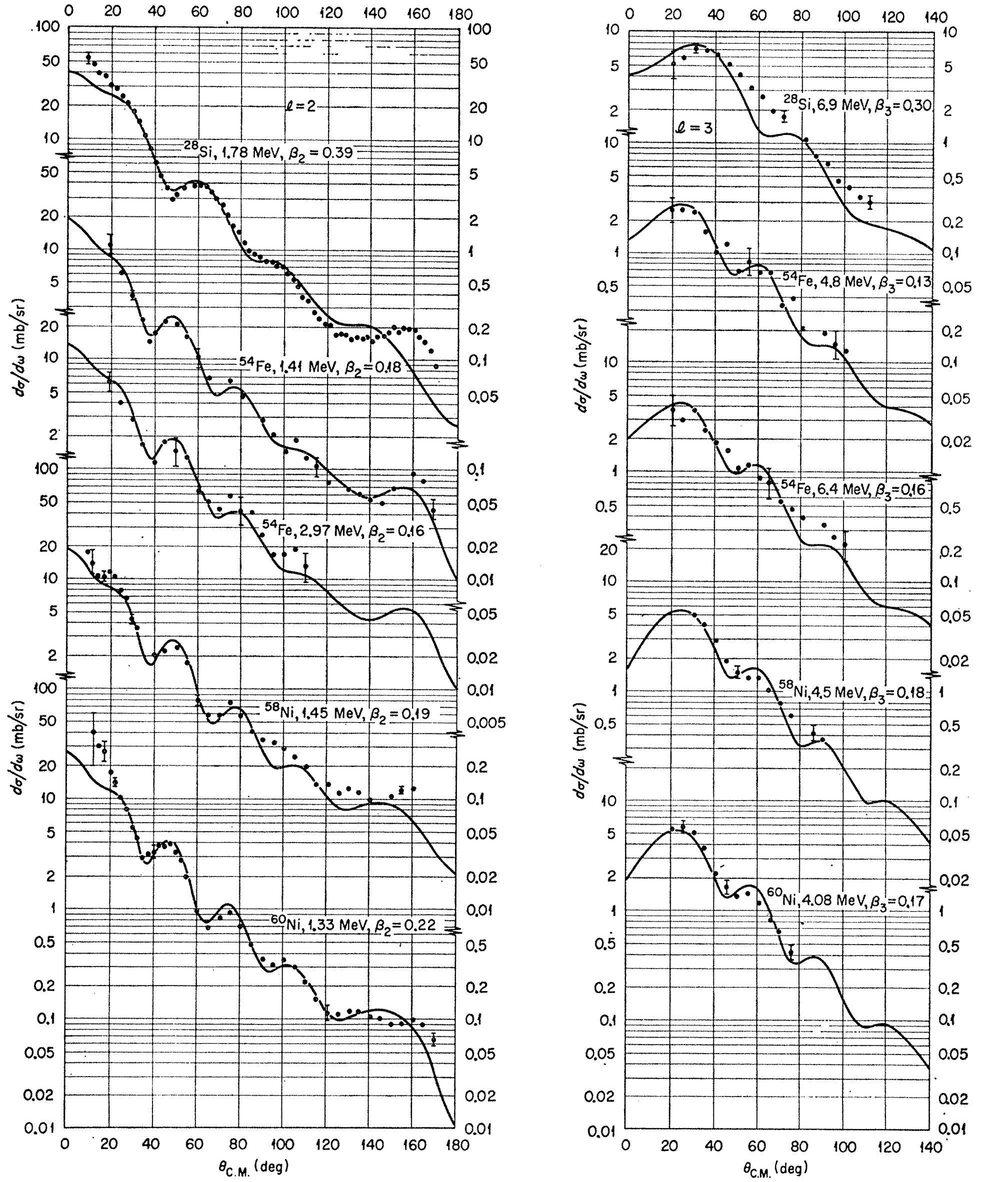

FIG. 10. Inelastic cross-section data and DW predictions using complex-plus-spin-orbit coupling and the optical-model parameters of Table II.

was mentioned, there is evidence from lower-energy work[14] that the asymmetries for some low-lying 2^+ states in medium-weight nuclei show differences which do not appear to be explained within the framework of the collective model. Some of these excitations are fairly enhanced and could be studied at higher energy with only a modest improvement in the resolution and intensity achieved here.

Our measurements of inelastic asymmetry have distinguished between some collective-model interactions believed plausible for the present data. In particular, we find the collective-model generalization of the optical model to be successful for these data only when the effective interaction is derived from both real and imaginary parts of the optical potential. Because the inelastic-asymmetry prediction is not insensitive to arbitrary variations in the imaginary form factor, the consistent improvement produced by the collective-model prescription for the imaginary interaction is indeed striking. For higher-energy proton scattering, the impulse approximation[35] also yields a complex-valued effective interaction; and it has been suggested[34] that a complex interaction may prove necessary in a microscopic treatment for medium-energy protons, as well as some two-body spin-orbit or tensor force.

The spin-dependent inelastic interaction of Eq. (11) has proved remarkably successful for both the inelastic

---

[35] R. M. Haybron and H. McManus, Phys. Rev. **140**, B638 (1965).

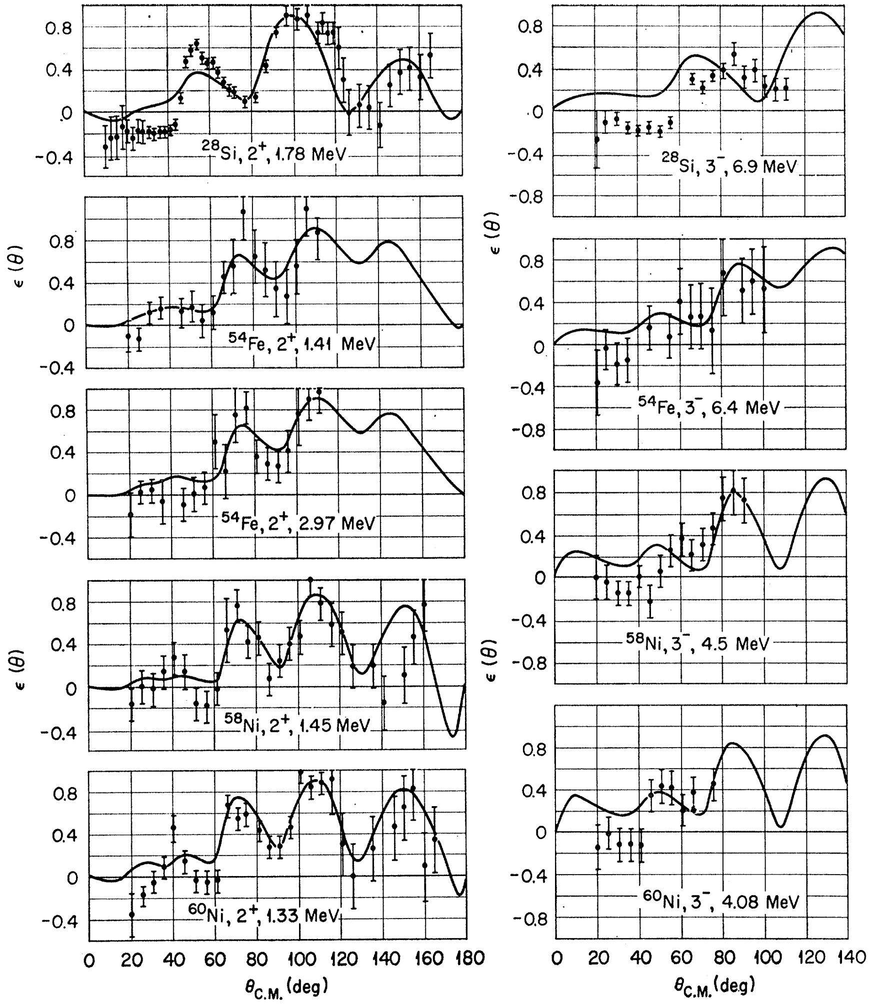

FIG. 11. Inelastic-asymmetry data and DW predictions using complex-plus-spin-orbit coupling and the optical-model parameters of Table II.

asymmetry and cross section at larger angles. But the poor agreement with the asymmetry data at foward angles suggests that the interaction is not yet complete. One might suspect that the proper collective interaction should also contain the more complicated terms which would arise from treating the form of the Thomas potential given in Eq. (13), but it is difficult to estimate the effect of these terms short of carrying out a full calculation. Such a study is now under way.[36] Alternatively, one could continue to examine the spin-dependent interaction phenomenologically. One possibility is to explore a different *radial* dependence for the spin-orbit interaction than is currently assumed for the elastic and inelastic scattering.

ACKNOWLEDGMENTS

We are indebted to R. M. Drisko for his computer programs and for his extensive guidance in their applications to these data. We have also benefited from a number of consultations concerning this analysis with R. H. Bassel and G. R. Satchler. We are grateful to B. J. Morton for much assistance in taking the data, and we thank the ORIC cyclotron operators and M. B. Marshall of the ORIC staff for their essential contributions to this experiment. It is a pleasure to acknowledge the continued support of this work by R. S. Livingston and A. H. Snell. We are grateful to T. Tamura and C. Y. Wong for furnishing the coupled-equations code. One of us (MPF) acknowledges the generous support of a graduate fellowship from the Oak Ridge Associated Universities.

---

[36] R. M. Drisko (private communication).